infrastructures

MDPI

Article

Surrogate-Assisted Cost Optimization for Post-Tensioned Concrete Slab Bridges

Lorena Yepes-Bellver [1,†], Alejandro Brun-Izquierdo [2], Julián Alcalá [3] and Víctor Yepes [3,*,†]

[1] Mechanics of Continuous Media and Theory of Structures Department, Universitat Politècnica de València, 46022 Valencia, Spain; loyebel@alumni.upv.es
[2] School of Civil Engineering, Universitat Politècnica de València, 46022 Valencia, Spain; albruiz@cam.upv.es
[3] Institute of Concrete Science and Technology (ICITECH), Universitat Politècnica de València, 46022 Valencia, Spain; jualgon@cst.upv.es
* Correspondence: vyepesp@cst.upv.es; Tel.: +34-96-387-9563
† These authors have made a joint and equitable contribution to the present study.

Abstract: The study uses surrogate modeling techniques to evaluate cost optimization methodologies for post-tensioned concrete slab bridges. These structures are key components in transportation infrastructure, where design efficiency can yield significant economic benefits. The research focuses on a three-span slab bridge, with spans of 24, 34, and 28 m, optimized through the Kriging surrogate model combined with heuristic algorithms such as simulated annealing. Input variables included deck depth, base geometry, and concrete grade, with Latin Hypercube Sampling ensuring diverse design exploration. Results reveal that the optimized design achieves a 6.54% cost reduction compared to conventional approaches, primarily by minimizing material usage—concrete by 14.8% and active steel by 11.25%. Among the predictive models analyzed, the neural network demonstrated the lowest prediction error but required multiple runs for stability, while the Kriging model offered accurate local optimum identification. This work highlights surrogate modeling as a practical and efficient tool for bridge design, reducing costs while adhering to structural and serviceability criteria. The methodology facilitates better-informed decision-making in structural engineering, supporting more economical bridge designs.

Keywords: bridges; concrete structures; heuristics; kriging; neural networks; optimization; structural design; surrogate models

Academic Editor: Darius Bačinskas

Received: 22 January 2025
Revised: 14 February 2025
Accepted: 17 February 2025
Published: 18 February 2025

Citation: Yepes-Bellver, L.; Brun-Izquierdo, A.; Alcalá, J.; Yepes, V. Surrogate-Assisted Cost Optimization for Post-Tensioned Concrete Slab Bridges. *Infrastructures* **2025**, *10*, 43. https://doi.org/10.3390/infrastructures10020043

1. Introduction

Both on roads and railway lines, overpasses are essential, and they are typically prestressed concrete (PC) bridges. These infrastructures represent a significant cost for the managers of such assets, ranging from 5% to 15% of the costs in these communication projects [1]. Therefore, designing the project as economically as possible is crucial, as the potential savings can be substantial. Optimization techniques are necessary to achieve this.

An overpass is usually designed as a continuous PC beam for spans ranging from 10 to 45 m. The structural advantages of these slab solutions make them competitive with precast beam bridges and construction benefits, as they adapt to complex layouts. The formwork and concreting process are simpler than other bridge types [2]. Additional

benefits include eliminating pavement joints, more flexible support placement, and improved aesthetics. The slab bridge balances construction ease and structural performance.

Slab bridges built in situ are cost-effective when complex geometric conditions, such as strong curvatures or varying widths, are involved or when reduced depths are required due to low road surface height. Conventional formwork is competitive for spans starting at 20 m. It is the standard method for slab bridges with up to four spans (below 120–140 m), as long as pile heights do not exceed 20 m. For longer spans, bridges are constructed in phases using conventional formwork. When pile height is significant, self-supporting and self-launching formwork is required to separate construction from the terrain.

For road overpasses, slab sections are often concreted in situ for typical spans of 30 m, reaching up to 60 m. For 40 m spans with continuous sections, the construction is competitive. Decks are typically reinforced concrete for bridges with spans under 15 m. Spans over 25 m often use variable sections or cantilevering. When the span exceeds 25 m and the deck depth remains constant, designers often lighten sections to reduce weight.

Engineers aim to design structures that are economical and resilient to natural hazards. Traditionally, these designs relied on trial and error, but optimization methods now offer a systematic approach to identify optimal solutions under specific constraints.

The foundations of mathematical optimization trace back to the 18th and 19th centuries with Lagrange and Euler, while Kantorovich and Dantzig developed mathematical programming principles in the 1940s. The computer revolution of the 1960s introduced heuristic optimization techniques that transformed problem-solving. However, advancements in bridge optimization were still needed. Research on bridge optimization began in the 1960s and 1970s, with Torres et al. [3] among the first to optimize concrete bridges. Early efforts focused on steel bridges, with only four articles on concrete bridge optimization published until the 1990s. Subsequently, research on both concrete and steel bridges advanced to reduce costs while meeting structural limit states. The first decade of the 21st century saw a significant increase in concrete bridge optimization publications.

Traditionally, the optimization of concrete slab bridges employed exact mathematical procedures, which were feasible only with limited design variables. Larger sets of variables increased computation times exponentially, necessitating simplifications such as limiting variables to active reinforcement [4] or section weight [5]. In these instances, passive reinforcement was excluded, and structural constraints were simplified to stresses in the section's extreme fibers [6,7]. Pioneering studies on slab bridge optimization used mathematical programming. Krisch [8] was the first to optimize a continuous slab bridge deck with four spans of varying lengths, defining the prestressing layout using linear programming based on eccentricity at equidistant sections. Afzal et al. [9] provide an update on concrete structure optimization.

The heuristic optimization of structures is computationally expensive [10], so metamodels like Kriging, artificial neural networks (ANNs), or radial basis functions (RBF) are used. This method replaces the simulation model, providing optimal interpolation by regression based on observed values [11]. Kriging has interesting applications, although its use in engineering real-world infrastructure is still limited [12]. Recently, it has been used to optimize aircraft structures made of composite materials [13], thin-walled structures [14], and reinforced concrete bridges [15–17]. Researchers use ANNs to predict structural behavior [18] and bridge conditions and risks [19].

Comparative studies on metamodel selection have not reached definitive conclusions about the superiority of any specific type [20,21]. Ryberg [22] notes that metamodel performance significantly depends on parameter tuning, which varies by software. Jin et al. [23] found that radial basis functions (RBFs) excel with small sample sets due to the ease of implementation and faster creation. Kriging achieves accuracy and robustness with larger sample sizes if well-calibrated. The authors consider RBF more reliable in most

cases. However, these studies face limitations, including reliance on reference functions, few variables, and fixed parameters affecting performance. Negrín et al. [24] present a recent review of metamodel-assisted optimization in structural engineering.

A cost optimization methodology is presented in this study for a PC slab bridge using the Kriging subrogated model. Unlike previous work focused on reducing CO_2 emissions [16] or embedded energy [17], this research aims to evaluate and compare the effectiveness of various approximate prediction models. The accuracy of the proposed method in complex design spaces may be affected by the quality of the sampled data. Although cost minimization is prioritized in this study, factors like environmental impact and maintenance are not explicitly considered. Furthermore, the heuristic optimization of the response surface generated by the metamodel, while not guaranteeing the global optimum, offers a good approximation from a practical point of view.

2. Three-Span Post-Tensioned Road Flyover Description

Engineers commonly use hyperstatic post-tensioned road flyovers for bridges between 10 m and 45 m long. However, when the main span exceeds 50 m, box girders offer a more competitive solution. Designers maintain a depth/span ratio of 1/25 for slabs with three or more spans. This design outperforms precast girders with higher bending stiffness, excellent durability, and enhanced safety from hyperstatic behavior. Additionally, its ability to adjust to intricate shapes simplifies formwork and concreting, improving efficiency. The design also eliminates joints and allows flexible pile placement, enhancing the visual appearance.

The research aims to enhance the 24–34–28 m road flyover design, commonly used over two-lane dual carriageways (Figure 1). The deck features a constant depth and a rectilinear design. As shown in Figure 2, the platform has a width of 8.30 m, with two 3.50 m lanes and 0.65 m of parapet on each side. The findings are directly relevant to the construction of bridges in practical settings.

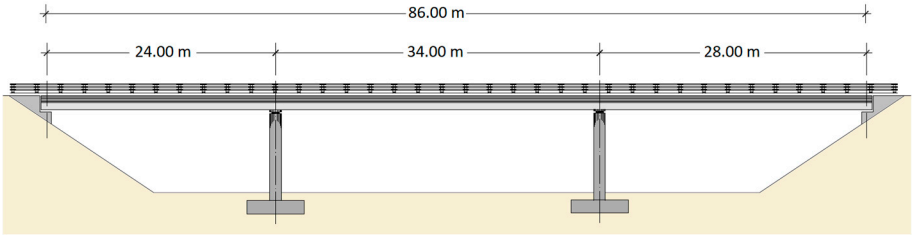

Figure 1. View of the longitudinal profile of the PC slab.

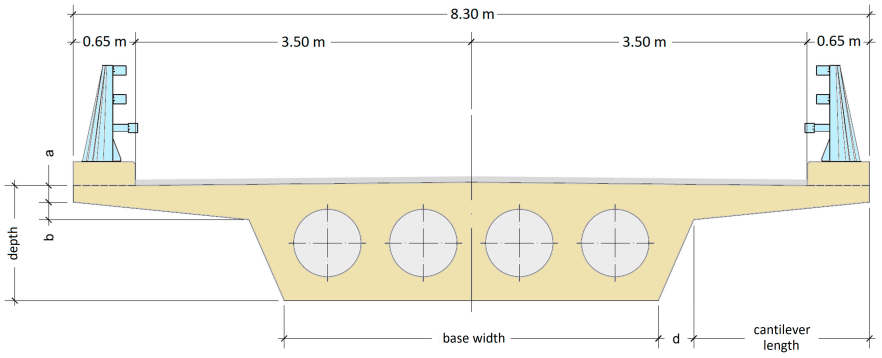

Figure 2. Cross-section of the lightweight PC slab bridge deck.

The flyover is located at the A-7 motorway in Cocentaina, Alicante. The design includes a 4.00 m base width, a depth of 1.35 m, and a 1.75 m lateral cantilever. The sizes are

as follows: a = 0.20 m, b = 0.10 m, and d = 0.40 m. The inner voids have four circular cylinders, each 0.60 m in diameter. These dimensions yield an internal void volume of 0.14 m^3/m^2. The external void volume is 0.51 m^3/m^2.

The passive steel is B-500S, consisting of longitudinal and transverse reinforcement. Longitudinal bars comprise a base standard to the deck and supplementary bars for bending and torsion in specific zones. The layout features five types of bars: bottom nucleus, top nucleus, top cantilever, bottom cantilever, and lateral web. Transverse bars include a core contour bar, an upper transverse bar, a lower cantilever bar, and shear stirrups on the webs of the sections. Reinforcement zones cover 70% of the span and 15% above the pier sections. Prestressing is constant throughout the deck. There are seven Y-1860 S7 steel strands with a diameter of 15.7 mm, uniformly distributed in the cross-section. There is a relationship between the number of tendons and webs in voided sections, linking prestressing to the cross-sectional geometry. The prestressing force is determined by balancing the self-weight of the structure with the required force. This force is defined by the tension before losses and the location of the anchor plates, which are the points where the force is transmitted to the structure. The curve friction coefficient indicates the tension loss per unit change in angle, while the parasitic friction coefficient accounts for the tension loss per unit length of the tendon. The wedge penetration represents the sliding of the tendon when released from the stressing jack. The values for these parameters have been obtained from recommended values for post-tensioning systems. Therefore, active and passive reinforcements are calculated once the geometrical parameters and the concrete grade are fixed, so they are not subject to optimization.

The structural constraints ensure compliance with serviceability and ultimate limit states defined in Eurocode 2, considering the actions specified in Eurocode 1, which include dead loads of 44 kN/m and the environmental exposure class of concrete XC4. They include bending, vertical, longitudinal, and punching shear; torsion; combined torsion with bending and shear; compression and tension stress; cracking; and vibration. Constructability and geometrical constraints are also checked for this structure type.

This research utilized CSiBridge version 21.0.0 software to develop a 3D model of the deck for analysis and dimensioning. Several alternatives were evaluated to obtain the stresses in each section. The structural analysis for each option calculates the acting stresses as section forces resulting from the mathematical model with the loads applied. Additionally, the analysis determines the stress resultants that each section resists. Stresses are calculated using a sectional approach to design each structural element. These force calculations correspond with those provided by Yepes-Bellver et al. [16,17].

3. Surrogate Modeling

Approximate models efficiently predict target responses based on design variables throughout the design space [25]. The process involves three stages: (a) obtaining the initial input dataset, (b) selecting the model type, and (c) selecting the fitting approach. The aim is to create a model that accurately forecasts the target response.

There has been a notable increase in the use of metamodels in structural optimization, particularly those based on Kriging methodologies [24]. Previously, ANNs were the most widely used technique. These two approaches remain the most complementary strategies, as confirmed by recent studies [16–23], which justify their selection in this work. Kriging provides exact predictions for training points and an explicit expression for optimization, while ANNs yield varying predictions, requiring multiple runs to stabilize results. These two approaches have been evaluated in this study, among other metamodels. Below is an overview of the approaches used in this study.

3.1. Kriging Metamodel

The Kriging approximation model estimates the value of an attribute at a point u based on a set of n values of z [26]. Here, the target response is the cost of the bridge deck. This method forecasts outputs without the need for extensive structural analysis. These surrogate models are deterministic, yielding consistent outputs for identical inputs lacking random error. The general formulation of a Kriging metamodel is as follows:

$$y(x) = f(x) + Z(x) \tag{1}$$

where $Z(x)$ is a stochastic, zero-mean spatially correlated residual modeled using a covariance function, and $f(\boldsymbol{x})$ is the approximation function analogous to a regression model. It consists of the deterministic trend component, often modeled as follows:

$$f(x) = \sum_{i=1}^{n} \beta_i f_i(x) \tag{2}$$

Here, $f_i(x)$ are the known basis functions (e.g., constant, linear, or quadratic), and β_i are unknown coefficients representing trend basis or mean, typically shown as a constant value (Ordinary Kriging), as zero (Simple Kriging), or as a polynomial model, such as a linear or quadratic model (Universal Kriging). Kriging models can be constructed using polynomial regressions of degrees zero, one, and two, designated in this study as Kriging 1, Kriging 2, and Kriging 3.

The above Kriging models are deterministic, meaning that the response from a model does not exhibit random error. In other words, repeated runs with the same input parameters yield the same response.

3.2. Artificial Neural Network

Neurons in input, hidden, and output layers comprise an ANN. Data are processed, and weights are adjusted iteratively using error backpropagation to improve accuracy. Hidden layer neurons connect to input and output layers. Input variables x_i are weighted by coefficients $w_{i,j}$, combined linearly with a bias term b_j. Each hidden neuron applies a sigmoid function, whereas the output layer uses a linear function for the final output.

The multilayer perceptron approximates functions with a single hidden layer [27], relying on the backpropagation algorithm [28–30]. In a forward-feeding network, connections flow in a single direction from input to output, employing supervised learning with data that have known responses. The data are separated into a training set, a validation set, and a test set to identify any cases of overfitting. Training data adjust parameters, validation data monitor overlearning, and test data evaluate performance. The "early stopping" method helps avoid overfitting by evaluating the errors in both training and validation datasets.

The neural network utilized 30 datasets: twenty-one for training, five for validation, and four for testing, selected randomly. The model includes a hidden layer with five neurons, and simulations evaluate performance using training or new prediction data. Cross-validation compares training outputs with simulated results, evaluating accuracy and detecting overfitting. Cross-validation can be utilized with training, validation, or test datasets.

3.3. Radial Basis Functions

Radial basis functions (RBFs) are interpolation and approximation methods widely used to construct surrogate models for complex systems [31]. They rely on radial symmetry, meaning the function's value depends only on the distance from a point of interest to a central point. RBFs are particularly effective for interpolating scattered data, offering

smooth, continuous approximations even in high-dimensional spaces. A radial basis function, with input variables x_i grouped in $\boldsymbol{x}$, can be expressed as

$$f(\boldsymbol{x}) = \sum_{i=1}^{N_\Phi} \Phi_i(\boldsymbol{x})\alpha_i + b(\boldsymbol{x}) \tag{3}$$

Here, $f = f(\boldsymbol{x})$ denotes the output response, $\Phi_i = \Phi_i(\boldsymbol{x})$ are the RBFs, N_Φ is the number of radial basis functions, α_i are the weights, and $b = b(\boldsymbol{x})$ is the bias term. The selection of the total count of radial basis functions matches the number of input variables.

The RBF choice (e.g., linear, Gaussian, and thin plate spline) influences the smoothness and flexibility of the model, with the most frequently used RBFs being as follows:

$$Linear: \Phi_i(r) = r \tag{4}$$

$$Multiquadratic: \Phi_i(r) = \sqrt{\left(\frac{r}{\varepsilon_i}\right)^2 + 1} \tag{5}$$

$$Inverse\ multiquadratic: \Phi_i(r) = \frac{1}{\sqrt{\left(\frac{r}{\varepsilon_i}\right)^2 + 1}} \tag{6}$$

$$Cubic: \Phi_i(r) = r^3 \tag{7}$$

Here, r is the Euclidean distance, and (ε_i) represents the shape parameter.

4. Methodology

This study analyzes the cost of each deck alternative and optimizes a Kriging response surface. The methodology follows a structured sequence to optimize the design process. It begins with selecting key design variables and determining their feasible ranges. Latin Hypercube Sampling (LHS) generates a representative set of design points. Each sample undergoes structural design and evaluation to ensure compliance with all constraints, followed by the computation of its cost function. A metamodel is then constructed to approximate the cost function, which is optimized to identify the optimal solution. Finally, the accuracy of the metamodel is assessed and, if necessary, refined iteratively until a satisfactory solution is achieved. The proposed methodology is summarized in Figure 3.

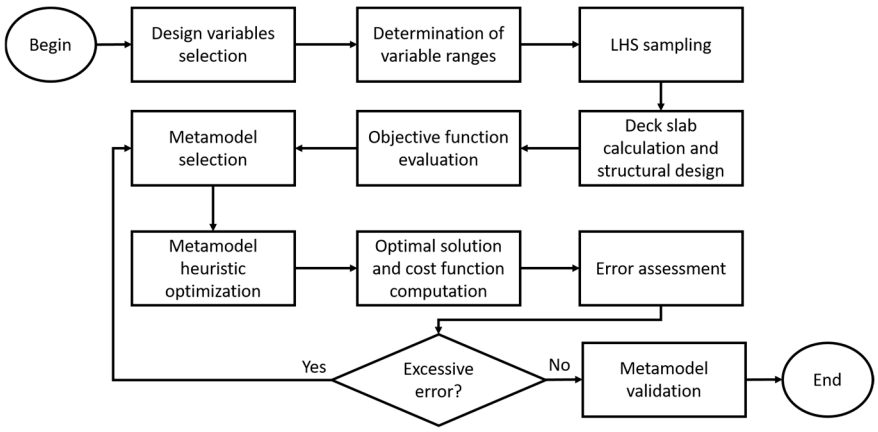

Figure 3. Simplified flowchart of the proposed methodology.

LHS selects random numbers that are uniformly distributed, providing lower sample mean variance than random sampling [32]. It samples intervals for each variable, running

the model for all intervals. LHS is flexible, efficiently adjusts sample sizes, and generates results quickly, making it widely applicable. Furthermore, LHS is one of the most commonly used techniques in surrogate modeling for structural applications [24].

LHS defines a set of geometric variables and concrete grades, generating different solutions. They include concrete strength in compression, slab depth, and base geometry. Once these variables are established, a complete structural analysis is conducted, including the design of active and passive reinforcements and verification of ultimate and serviceability limit states. This ensures that each solution complies with safety and serviceability requirements. After sizing the structure, the measurements of the units are determined, allowing for cost estimation. This methodology guarantees that all sampled solutions are viable and meet regulatory standards. Note that the proposed method optimizes the response surface instead of optimizing all of the structure variables.

4.1. Cost Evaluation

Each slab deck construction involves costs analyzed through concrete grade, steel quantity, formwork surface, and lighting. The BEDEC database [33] provides the unit costs shown in Table 1, a widely recognized resource among national contractors, ensuring a realistic cost analysis. While these market prices naturally vary depending on economic conditions and local factors, this does not affect the general applicability of the proposed methodology. The unit costs that multiply the measurements serve as the weights of the objective function.

Table 1. Deck unit costs.

Deck Unit	Cost (EUR)
kg B-500-St steel	1.16
kg Y-1860-S7 steel	3.40
m^3 C-30 concrete	99.81
m^3 C-35 concrete	104.57
m^3 C-40 concrete	109.33
m^3 C-45 concrete	114.10
m^3 C-50 concrete	118.87
m^3 voids	99.81
m^2 formwork	33.81

Cost relates to measuring each material. The cost of the materials used is considered as it differentiates the options. At this stage, the study of a conventional solution would generally close with selecting the lowest cost deck. Nevertheless, a methodology that can lower costs by applying optimization to a Kriging model using the set of alternatives obtained from sampling is suggested.

4.2. Sampling and Data Collection

The points' number and location determine the sampling. Sample size correlates with variable count for similar metamodel accuracy. A sample size of approximately 30 individuals for concrete structures yields favorable results [16,17]. Random values from 0 to 1 correspond to each parameter modified after LHS. Next, values fit predefined variable ranges and adjust within them, producing solutions. This approach generates designs that meet optimization model inputs, undergo structural analysis, and observe with Limit States to ensure a buildable bridge.

LHS sampling diversifies the exploration for the locally optimal solution. Variables include concrete strength in compression, slab depth, and base geometry. Concrete strength varies between 30 and 50 MPa, depth from 1.15 to 1.70 m, and base from 3.00 to

5.00 m in 5 cm increments. Minimum coating is the distance between voids or from voids to the deck face. After determining variables, LHS sampling generates combinations for the metamodel, ranging from 0 to 1. Edge and bottom base dimensions are multiples of 5 cm, and concrete strength values are integer multiples of five.

The maximum number of voids corresponds to the highest possible number that can be accommodated within the section. Table 2 presents the dimensional ranges and their constraints as the General Directorate of Public Roads of Spain [34] recommended. The minimum coating refers to the shortest distance between a void and the deck surface or adjacent voids.

Table 2. Dimensional ranges and their constraints as recommended by [34].

Design Variables	Range	Limitation
Concrete grade (f_{ck})	30–50 MPa	-
Deck depth (c)	1.15–1.70 m	>0.90 m
Base width (b)	3.00–5.00 m	-
Cantilever length (v)	Variable	<3.50 m
Distance between cantilever and nucleus (d)	0.40 m	-
Cantilever starting thickness e_1 ($a + b$)	0.35 m	-
Cantilever edge thickness e_2 (a)	0.25 m	>0.20 m
Minimum void coating	0.225 m	>0.15 m

In Table 3, deck depth, base width, and concrete grade are metamodel inputs, while cost is output.

Table 3. Design variables in the defined ranges.

Deck	Deck Depth (m)	Base Width (m)	Concrete Grade (MPa)	Cost (EUR)
1	1.45	4.35	35	192,057.24
2	1.55	4.10	35	205,791.78
3	1.45	4.75	35	197,491.93
4	1.70	3.80	45	208,483.87
5	1.20	3.85	40	184,075.17
6	1.55	3.60	45	189,644.46
7	1.20	4.85	50	196,809.28
8	1.15	4.50	50	195,215.52
9	1.35	3.95	30	187,145.69
10	1.30	4.45	30	195,251.53
11	1.35	4.25	45	194,435.77
12	1.50	4.55	30	192,497.60
13	1.60	4.20	40	199,854.38
14	1.25	4.70	40	194,671.69
15	1.50	4.05	45	193,285.15
16	1.30	4.90	40	197,991.85
17	1.65	3.65	35	190,969.37
18	1.65	3.45	45	191,799.47
19	1.25	3.50	45	181,265.33
20	1.40	3.30	40	181,320.82
21	1.45	3.90	45	194,740.91
22	1.35	3.60	35	186,808.36
23	1.60	3.35	45	190,539.61
24	1.50	4.50	45	202,670.58
25	1.55	3.20	30	182,398.13
26	1.25	3.00	50	181,043.85
27	1.40	3.45	45	186,143.08
28	1.50	3.55	35	185,779.65
29	1.70	3.85	40	198,548.66
30	1.15	3.70	40	182,731.07

The methodology differs from traditional analysis by using LHS sampling to fit a Kriging model optimized with a heuristic algorithm. Heuristic algorithms apply AI techniques to select designs, analyze structures, check constraints, and modify variables iteratively to optimize the objective function. While they do not guarantee a global optimum, they deliver near-optimal solutions in a reasonable time. Structural complexity often requires heuristic optimization, though it can be time-consuming. Surrogate models like polynomial regression, neural networks, or Kriging provide faster approximate responses than the actual model to reduce computational cost. Figure 4 shows the cost response surface depending on the concrete grade and the depth of the deck, with a steep surface featuring peaks and valleys due to the nonlinearities and interactions among design parameters. LHS chooses random numbers that are uniformly distributed to evaluate cost alternatives. Subsequently, an approximate Kriging model generates and optimizes a response surface created with the input data.

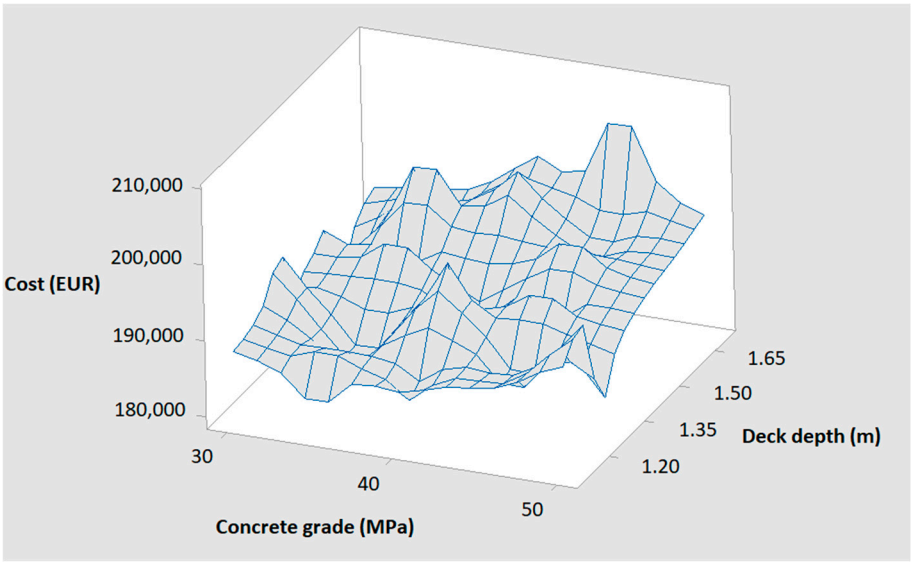

Figure 4. Response surface of cost depending on concrete grade and deck depth (Tables 3 and 4).

4.3. Response Surface Optimization Approach

The MATLAB Kriging Toolbox (DACE) constructed a surrogate model from computer experiment data, approximating the original model. A computer experiment involves input–response pairs from model simulations to derive a response surface for optimization. The DACE documentation outlines the mathematical framework for the Version 2.0 toolbox [35].

This study used simulated annealing as a heuristic algorithm [36], miming how crystal molecules reach minimum energy. Solutions are accepted based on $\exp(-\Delta E/T)$. Here, ΔE indicates the growth of the objective function, and T is a parameter. This allows accepting worse solutions to escape local optima, allowing for an extensive search for the global optimal solution. The initial temperature T_0 is set using Medina's method [37] and adjusted by the acceptance ratio. Temperatures reduce geometrically every 1000 Markov chains with a cooling factor $k = 0.8$, lowering the likelihood of accepting worse solutions.

A conventional study would select deck #30 (Table 2) as it has the lowest cost. However, optimizing a Kriging model aims to identify a lower-cost solution than the sample. After optimizing the metamodel using simulated annealing, the optimized deck has a depth of 1.30 m and a base width of 3.15 m. After optimization, the cost for the bridge deck is EUR 180,071.26.

The optimized deck features a volume of 434.91 m^3 of C-35 concrete, 52,468.53 kg of B-500-S steel, 10,538.13 kg of Y-1860-S steel, 865.69 m^2 of slab formwork, and 86.25 m^3 of

voids. These measurements cost EUR 2093.85 per meter of bridge length and EUR 252.27 per square meter of bridge deck. The original deck, with a base width of 4.00 m, a depth of 1.35 m, and a C-35 concrete grade, costs EUR 192,665.98. The optimized bridge is 6.54% more cost-effective than the original bridge. The optimized bridge uses 14.80% less concrete and 11.25% less active steel, with the remaining measurements similar to the original design.

Figure 5 presents the normalized measurements and costs of the optimized structure relative to the reference slab. A significant reduction can be observed in the quantities of concrete, prestressed reinforcement, and overall cost. However, the amounts of passive steel, voids, and formwork have no significant variations.

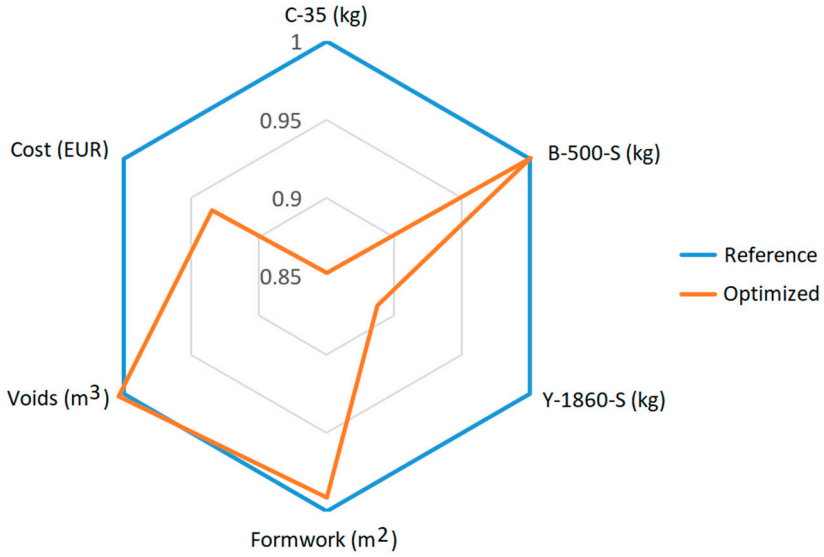

Figure 5. Normalized measurements and costs of the optimized structure relative to the reference slab.

Although this cost reduction is moderately lower than achieved with the complete heuristic optimization of all structural variables, the proposed methodology offers a simpler alternative by optimizing the response surface rather than the entire structure. For instance, Martí et al. [38] reported cost savings of approximately 8% in precast PC road bridges using simulated annealing. However, our approach requires less computational effort while significantly reducing material consumption.

5. Results and Discussion

This section compares the performance of several prediction models by examining discrepancies between the known values of new solutions and the predictions. The models were fitted using the first 30 data points from Table 3. Real decks #31 to #38 were then used for a mean square error (MSE) analysis (Table 4). These new decks are unknown to the models, making them helpful in assessing prediction errors. Solution #38, which represents the optimal result from the Kriging-generated surface, is also highlighted.

After fitting a metamodel, the RMSE (root mean square error) can assess the prediction error.

$$RMSE = \sqrt{\sum_{i=1}^{n} \frac{(\hat{y}_i - y_i)^2}{n}} \quad (8)$$

where $\hat{y}_i$ are the predicted values, y_i are the known values, and n is the number of observations.

Table 4. Additional design variable values obtained within the defined ranges.

Deck	Deck Depth (m)	Base Width (m)	Concrete Grade (MPa)	Cost (EUR)
31	1.15	3.40	35	189,650.53
32	1.25	3.35	35	181,823.43
33	1.15	3.65	45	187,493.16
34	1.15	3.35	40	180,205.16
35	1.15	3.25	40	180,886.29
36	1.15	3.55	40	190,063.83
37	1.10	3.40	35	181,530.72
38	1.30	3.15	35	180,071.26

5.1. Visualization of Observed Data

A response surface can be plotted with observed data using Minitab v17 before using the metamodels. Figures 6 and 7 display the 38 observed data points (Tables 3 and 4), with cost as output. Figure 7 presents the contour plot of the observed data, showing several peaks and valleys. The response surface is abrupt, and evaluating which types of surrogate models are most suitable for predicting and optimizing the solution within this space is necessary.

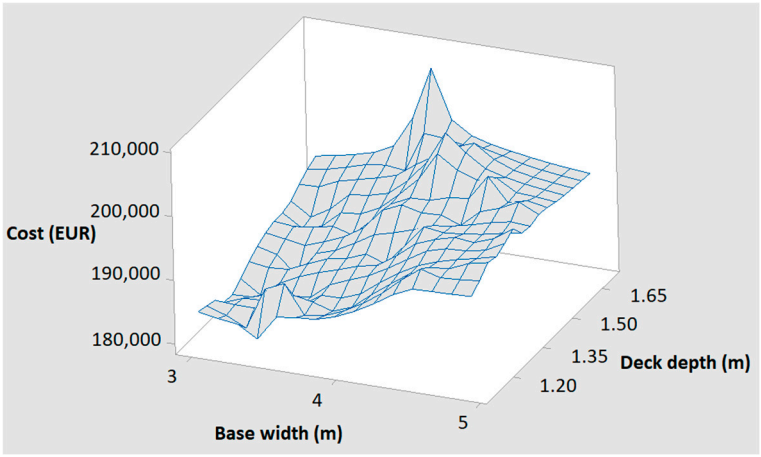

Figure 6. Response surface for the 38 observed deck data points (Tables 3 and 4).

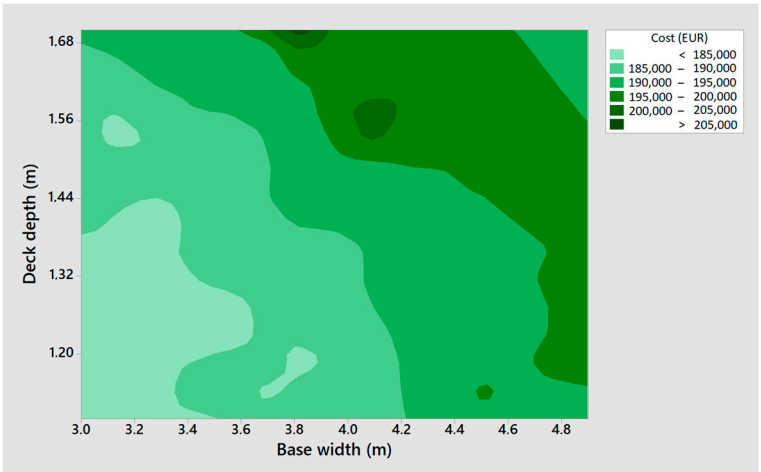

Figure 7. Contour plot for the 38 observed deck data points (Tables 3 and 4).

Surrogate models do not always capture the nuances of local optima in response surfaces with abrupt features, like those shown in Figures 6 and 7. Figure 8 displays the quadratic polynomial model fitted to the 30 data points from Table 3. While this model predicts a minimum close to that of the response surface, it has significantly smoothed the response. However, these simple polynomial models allow for studying trends in some problems.

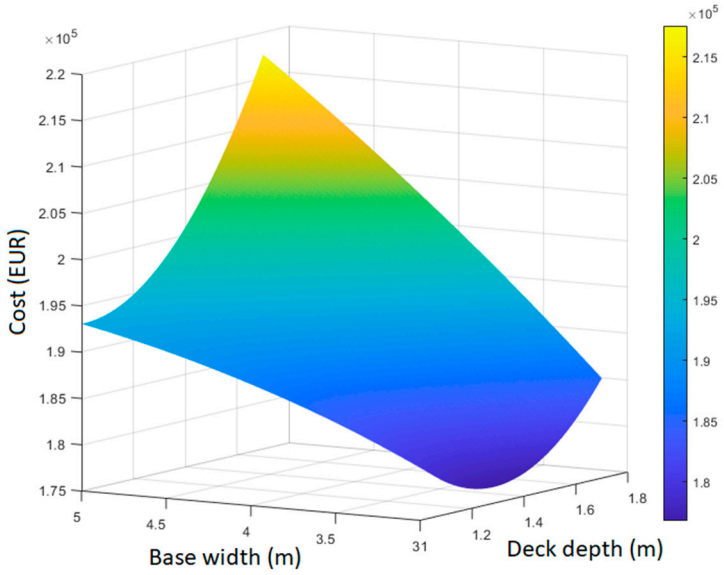

Figure 8. Polynomial quadratic model fitted at 30 observed slab bridge deck data points (Table 2).

The linear and quadratic polynomial models fitted to the 30 points in Table 3 are shown in Equation (9) and Equation (10), respectively. In these expressions, the response variable y represents the cost (EUR), x_1 is the deck depth (m), x_2 is the base width (m), and x_3 is the concrete grade (MPa).

$$y = 93242.77 + 28831.54x_1 + 11271.66x_2 + 322.77x_3 \quad (9)$$

$$y = 389214.11 - 224420.62x_1 - 5097.12x_2 - 3969.32x_3 + 51646.58x_1^2 - 1158.79x_2^2 + 23.45x_3^2 + 13971.64x_1x_2 + 1252.19x_1x_3 + 161.92x_2x_3 \quad (10)$$

5.2. Prediction Models Comparison

Table 5 presents the observed values, the polynomial fitting, Kriging, RBF, and the average results from 16 ANN runs for deck #38 in the response surface optimization. Note that neural networks are not deterministic, as the data for learning and validation is randomly selected each time. Consequently, the ANN was run several times to stabilize the standard deviation of the means.

Table 5. Absolute and relative errors for local optima (#38).

	#38	Absolute Error	Relative Error
Observed	180,071.26	0.00	0.00%
Linear	177,526.45	−2544.81	−1.41%
Quadratic	179,036.24	179,036.24	−0.57%
Kriging 1	182,928.86	2857.60	1.59%
Kriging 2	177,218.88	−2852.38	−1.58%
Kriging 3	179,032.11	−1039.15	−0.58%
Linear RBF	183,589.60	3518.34	1.95%
Multiquadratic RBF	170,870.73	−9200.53	−5.11%

Inverse Multiquadratic RBF	163,652.53	−16,418.73	−9.12%
Cubic RBF	169,577.93	−10,493.33	−5.83%
ANN average	180,010.27	−60.99	−0.03%

The average values predicted by ANN provide the lowest error. In addition, the Kriging 3, which employs an order 2 regression polynomial, gives an error close to that of the quadratic polynomial model. Nevertheless, the MSE and RMSE errors are lower for the polynomial quadratic and Kriging 3 models than in the ANN case (Table 6). These errors were obtained from predicting values #31 to #38.

Table 6. MSE and RMSE of the models employed.

Models	**MSE**	**RMSE**
Linear	53,978,296.90	7346.99
Quadratic	14,069,613.95	3750.95
Kriging 1	18,928,756.82	4350.72
Kriging 2	51,358,533.85	7166.49
Kriging 3	14,100,395.62	3755.05
Linear RBF	18,152,649.81	4260.59
Multiquadratic RBF	57,938,931.10	7611.76
Inverse multiquadratic RBF	122,086,223.32	11,049.26
Cubic RBF	56,608,633.18	7523.87
ANN average	20,824,711.27	4563.41

This analysis verifies the good performance of ANNs in predicting the optimal value. The next step thoroughly examines the ANN's ability to identify optimal values. Therefore, this model will be analyzed to assess how the response surface behaves around the localized optimum by optimizing the response surface (deck #38). ANNs were used to analyze the behavior of solutions around the optimal cost solution. This approach has allowed us to verify that the optimal solution identified by optimizing the Kriging metamodel is consistent with the behavior predicted by the ANNs in the neighborhood of the optimum. The average prediction values, shown in Figures 8–10 below, illustrate this.

Figure 9 shows the ANN's accurate minimum slab depth prediction based on a 3.15 m base and 35 MPa concrete grade. A minimal value occurs at 1.20 m, closely matching the optimum value determined by Kriging.

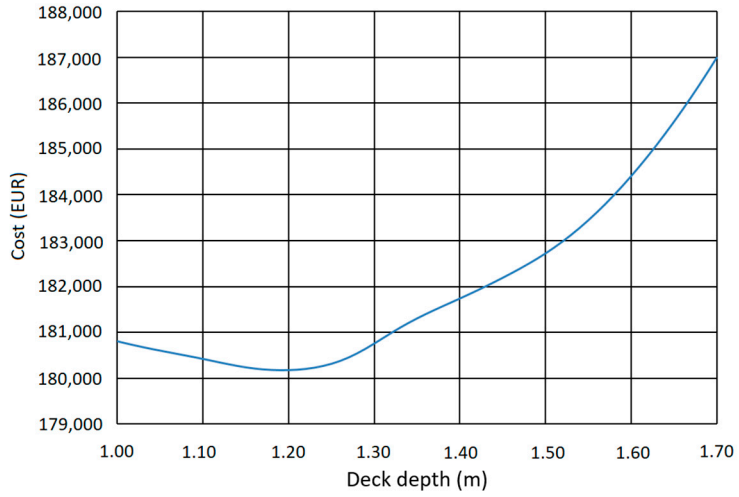

Figure 9. ANN cost for a 3.15 m base width and 35 MPa concrete grade as a function of deck depth.

For a slab depth of 1.30 m and a concrete strength of 35 MPa, the ANN suggests (Figure 10) that the cost decreases as the slab width increases. This prediction aligns with the optimum found by Kriging, whose base width value was 3.15 m.

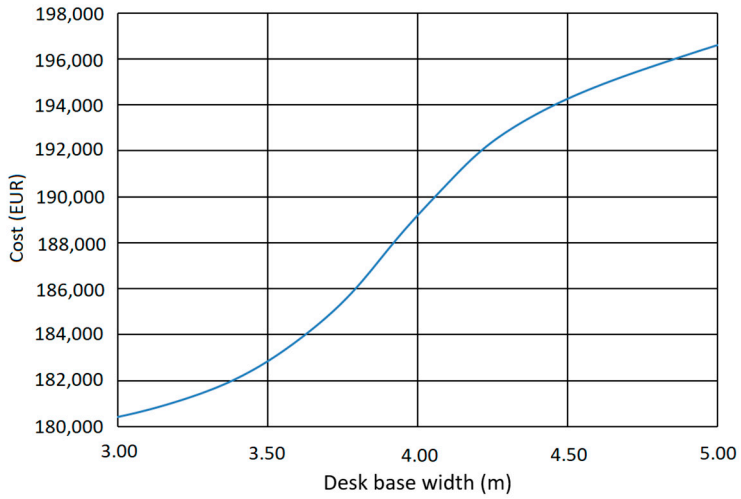

Figure 10. ANN cost for a 1.30 m depth and 35 MPa concrete grade as a function of deck depth width.

Considering a 1.30 m deck depth and a base of 3.15 m, Figure 11 shows that the ANN suggests that the characteristic resistance value that minimizes the cost is just above 35 MPa, similar to the value obtained in the optimization.

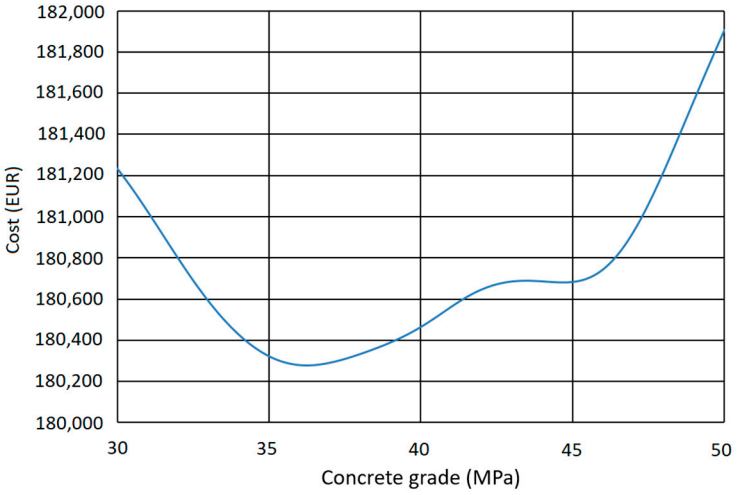

Figure 11. ANN cost for a 1.30 m depth and 3.15 m base width as a function of the concrete grade.

The ANN local optimum is very similar to the Kriging local optimum. All metamodels should accurately predict costs, and optimizing the response surface to identify a local minimum is essential. This approach benefits structural engineers, who typically avoid heuristic optimization algorithms and miss opportunities to reduce costs. It supports achieving more efficient, cost-effective designs.

The surrogate model methodology applies to all parameterized structures, enabling more efficient designs by adjusting key cost-influencing parameters.

Though it may seem like excessive work for deck cost reduction, working with parameterized structures allows for programming data inputs into calculation software, saving time on structure verification for each individual in the analyzed population.

Additionally, this methodology can precisely estimate future deck costs before calculating road overpasses with narrow load and dimension ranges, offering a significant advantage during the solution study phase.

5.3. Recommendations for Practical Use

The General Directorate of Public Roads of Spain (DGC) [34] recommends an optimum ratio of deck depth to main span between 1/22 and 1/30. In contrast, the SETRA [39] suggests a ratio of 1/28 specifically for three-span concrete decks with lateral cantilevers. These guidelines provide slenderness near 1/28, a concrete content between 0.55 m^3/m^2 and 0.60 m^3/m^2 for the deck, and a passive steel ranging from 100 kg/m^3 to 130 kg/m^3. The active steel should be approximately 17 kg/m^2 of the deck. The concrete grade should be at least 40 MPa.

In the context of cost optimization, it is noted that for a PC slab bridge with a 34 m main span, the concrete grade can be lowered to 35 MPa. The slenderness ratio found for the optimum cost, 1/26.15, also falls within the recommended ranges outlined earlier. This result demonstrates that the selected design minimizes costs while adhering to established guidelines, ensuring structural efficiency and compliance with best practices.

Yepes et al. [1] compare the optimal bridge to the statistical study on 61 real post-tensioned slab bridges. Table 7 presents basic statistics for lightweight slab decks, including the mean, coefficient of variation, minimum, maximum, 25th, 50th, and 75th percentiles. The average span-to-depth ratio is 23.93. For the optimized deck, with spans of 24, 34, and 28 m, ratios range from 18.46 to 26.15, within the 25th to 75th percentile range for PC slab decks. Considering the concrete volume per square meter (m^3/m^2), the ratio is 0.61, 6.56% lower than the mean (0.65). The passive reinforcement ratio is 73.53, 13.26% higher than the mean. The ratio for active reinforcement (kg/m^2) is 14.76, slightly below the first quartile. The optimized deck cost is 252.27 EUR/m^2, below the 25th percentile. This comparison shows the bridge deck falls within the range of PC slab decks in Spain. Therefore, the cost-optimal solution has a lower concrete volume and active reinforcement, compensated by a higher passive reinforcement ratio. Additionally, its cost below the 25th percentile highlights designers' limited use of optimization techniques.

Table 7. Slab deck variables from a sample of 61 individuals [1].

	Mean	C.V.	Min	Max	P 25	P 50	P 75
Total length (m)	91.87	60.7%	22.18	300.20	60.50	72.00	92.40
Width deck (m)	11.42	24.5%	7.60	23.00	9.90	11.00	12.45
Main span (m)	29.97	20.6%	18.00	45.00	25.00	31.00	35.48
Depth deck (m)	1.25	14.2%	0.85	1.75	1.13	1.25	1.32
Main span/depth deck	23.93	12.0%	18.46	30.40	21.74	23.33	26.39
Concrete (m^3/m^2)	0.65	17.3%	0.44	0.97	0.56	0.66	0.71
Steel prestressed (kg/m^2)	22.64	28.9%	11.17	38.16	17.99	21.99	26.85
Steel reinforcement (kg/m^2)	64.92	14.9%	42.80	92.91	57.76	65.27	69.91
External voids (m^3/m^2)	0.40	30.8%	0.12	0.74	0.31	0.39	0.47
Internal voids (m^3/m^2)	0.20	24.2%	0.11	0.33	0.16	0.20	0.24
Formwork (m^2/m^2)	1.12	3.9%	1.01	1.23	1.09	1.12	1.15
Desk cost (€/m^2)	314.10	15.2%	228.72	436.36	276.67	317.27	346.73

6. Conclusions

This paper validates a Kriging-based model for cost optimization in designing post-tensioned concrete slab bridges. By combining Kriging models with Latin Hypercube Sampling (LHS) and simulated annealing algorithms, the optimization process achieved a 6.54% reduction in total bridge deck cost compared to traditional methods. This result stems from a 14.8% decrease in concrete volume and an 11.25% reduction in active steel, highlighting the methodology's efficiency in conserving materials without compromising structural performance.

The comparative analysis of predictive models shows that Kriging with second-order polynomials provides a robust framework for identifying local optima in complex design spaces. At the same time, artificial neural networks (ANNs) offer high predictive accuracy

at the cost of computational intensity due to iterative convergence. Although computationally efficient, radial basis functions (RBFs) struggle with the steep, multi-dimensional response surfaces characteristic of this study.

The optimized design meets practical engineering standards, including recommended slenderness ratios and material configurations, ensuring compliance with serviceability and ultimate limit states. The findings also indicate that surrogate models are tools for predicting optimal solutions and facilitate the systematic exploration of design parameters, providing insights into trade-offs that inform decision-making.

From a practical perspective, integrating surrogate-assisted optimization into routine bridge design workflows can significantly reduce costs. This methodology enables early-stage cost prediction and tailored solutions for complex geometric or material constraints. Expanding this framework to other structural types promises similar benefits, especially in high-stakes infrastructure projects.

Despite its effectiveness, the methodology relies on sampled data quality, which affects accuracy in complex design spaces. While cost minimization is prioritized, environmental impact and maintenance are not explicitly considered. Heuristic optimization does not ensure a global optimum but provides a practical approximation.

Future research should explore alternative concrete types, such as high-strength concrete and fiber-reinforced concrete, to enhance structural performance and cost efficiency, as well as other types of bridges used as motorway overpasses. Additionally, multicriteria decision-making techniques using metamodels and response surfaces with multiple outputs could incorporate other relevant criteria, such as minimizing greenhouse gas emissions, durability, and maintenance.

Author Contributions: This paper represents a result of teamwork. Conceptualization, L.Y.-B., A.B.-I. and V.Y.; methodology, L.Y.-B., A.B.-I. and V.Y.; software, L.Y.-B. and J.A.; validation, L.Y.-B., A.B.-I. and J.A.; formal analysis, L.Y.-B., A.B.-I. and J.A.; investigation, L.Y.-B., A.B.-I., J.A. and V.Y.; resources, V.Y.; data curation, L.Y.-B. and A.B.-I.; writing—original draft preparation, L.Y.-B.; writing—review and editing, V.Y.; visualization, L.Y.-B. and A.B.-I.; supervision, J.A. and V.Y.; project administration, V.Y.; funding acquisition, V.Y. All authors have read and agreed to the published version of the manuscript.

Funding: Grant PID2023-150003OB-I00 funded by MCIN/AEI/10.13039/501100011033 and by "ERDF A way of making Europe".

Institutional Review Deck Statement: Not applicable.

Informed Consent Statement: Not applicable.

Data Availability Statement: Data are contained within the article.

Acknowledgments: The authors are grateful to the anonymous reviewers for their valuable contributions to improving the earlier version of this manuscript.

Conflicts of Interest: The authors declare no conflicts of interest.

References

1. Yepes, V.; Díaz, J.; González-Vidosa, F.; Alcalá, J. Statistical characterization of prestressed concrete road bridge decks. *Rev. Constr.* **2009**, *8*, 95–109. Available online: https://repositorio.uc.cl/handle/11534/11437 (accessed on 13 January 2025).
2. Aparicio, A.C.; Estradera, J.M. Aplicación del método de elementos finitos al estudio de la distorsión de tableros de puente de sección losa aligerada. *Rev. Int. Metodos Numer. Calc. Diseno Ing.* **1985**, *1*, 3–26. Available online: https://raco.cat/index.php/RevistaMetodosNumericos/article/view/68325 (accessed on 16 January 2025).
3. Torres, G.G.B.; Brotchie, J.F.; Cornel, C.A. A program for the optimum design of prestressed concrete highway bridges. *PCI J.* **1966**, *10*, 63–71. https://doi.org/10.15554/pcij.06011966.63.71.

4. Azad, A.K.; Qureshi, M.A. Optimum post-tensioning for three-span continuous slab-type bridge decks. *Eng. Optim.* **1999**, *31*, 679–693. https://doi.org/10.1080/03052159908941392.
5. Utrilla, M.A.; Samartín, A. Optimized design of the prestress in continuous bridge decks. *Comput. Struct.* **1997**, *64*, 719–728. https://doi.org/10.1016/S0045-7949(96)00434-8.
6. Lounis, Z.; Cohn, M.Z. Multiobjective optimization of prestressed concrete structures. *J. Struct. Eng.* **1993**, *119*, 794–808. https://doi.org/10.1061/(ASCE)0733-9445(1993)119:3(794).
7. Cohn, M.Z.; Dinovitzer, A.S. Application of structural optimization. *J. Struct. Eng.* **1994**, *120*, 617–649. https://doi.org/10.1061/(ASCE)0733-9445(1994)120:2(617).
8. Krisch, U. Optimized prestressing by linear programming. *Int. J. Numer. Methods Eng.* **1973**, *7*, 125–136. https://doi.org/10.1002/nme.1620070202.
9. Afzal, M.; Liu, Y.; Cheng, J.C.P.; Gan, V.J.L. Reinforced concrete structural design optimization: A critical review. *J. Clean. Prod.* **2020**, *260*, 120623. https://doi.org/10.1016/j.jclepro.2020.120623.
10. Carbonell, A.; González-Vidosa, F.; Yepes, V. Design of Reinforced Concrete Road Vaults by Heuristic Optimization. *Adv. Eng. Softw.* **2011**, *42*, 151–159. https://doi.org/10.1016/j.advengsoft.2011.01.002.
11. Cressie, N. The origins of Kriging. *Math. Geol.* **1990**, *22*, 239–252. https://doi.org/10.1007/BF00889887.
12. Martínez-Frutos, J.; Martí, P. Diseño óptimo robusto utilizando modelos Kriging: Aplicación al diseño óptimo robusto de estructuras articuladas. *Rev. Int. Métodos Numér. Cálc. Diseño Ing.* **2014**, *30*, 97–105. https://doi.org/10.1016/j.rimni.2013.01.003.
13. de Souza Mello, F.M.; Gomes, G.F. Sensor Placement Optimization for Composite Aircraft Structures: A Multi-Objective Kriging-Based Approach. *Compos. Struct.* **2025**, *353*, 118723. https://doi.org/10.1016/j.compstruct.2024.118723.
14. Hua, Y.; Gao, J.; Zhao, H.; Zhu, W. A Configuration-Driven Modal Optimization Method for Thin-Walled Structures Using a Surrogate-Assisted Evolutionary Algorithm with an Iterative Update Kriging Model. *Eng. Struct.* **2025**, *322*, 119182. https://doi.org/10.1016/j.engstruct.2024.119182.
15. Godin-Hebert, E.; Khorramian, K.; Oudah, F. Recommendations for Active-Learning Kriging Reliability Analysis of Bridge Structures. *J. Bridge Eng.* **2025**, *30*, 04024099. https://doi.org/10.1061/JBENF2.BEENG-6697.
16. Yepes-Bellver, L.; Brun-Izquierdo, A.; Alcalá, J.; Yepes, V. CO2-optimization of post-tensioned concrete slab-bridge decks using surrogate modeling. *Materials* **2022**, *15*, 4776. https://doi.org/10.3390/ma15144776.
17. Yepes-Bellver, L.; Brun-Izquierdo, A.; Alcalá, J.; Yepes, V. Embodied energy optimization of prestressed concrete road flyovers by a two-phase Kriging surrogate model. *Materials* **2023**, *16*, 6767. https://doi.org/10.3390/ma16206767.
18. Martí-Vargas, J.R.; Ferri, F.J.; Yepes, V. Prediction of the transfer length of prestressing strands with neural networks. *Comput. Concr.* **2013**, *12*, 187–209. https://doi.org/10.12989/cac.2013.12.2.187.
19. Principi, L.; Morici, M.; Natali, A.; Salvatore, W.; Dall'Asta, A. Preliminary Fast Assessment of Bridge Risk by Neural Network. *Int. J. Disaster Risk Reduct.* **2025**, *116*, 105084. https://doi.org/10.1016/j.ijdrr.2024.105084.
20. Kim, B.-S.; Lee, Y.-B.; Choi, D.-H. Comparison study on the accuracy of metamodeling technique for non-convex functions. *J. Mech. Sci. Technol.* **2009**, *23*, 1175–1181. https://doi.org/10.1007/s12206-008-1201-3.
21. Li, Y.F.; Ng, S.H.; Xie, M. A systematic comparison of metamodeling techniques for simulation optimization in decision support systems. *Appl. Soft Comput.* **2010**, *10*, 1257–1273. https://doi.org/10.1016/j.asoc.2009.11.034.
22. Ryberg, A. Metamodel-Based Design Optimization—A Multidisciplinary Approach for Automotive Structures. 2013. Available online: https://liu.diva-portal.org/smash/get/diva2:601789/FULLTEXT01.pdf (accessed on 16 January 2025).
23. Jin, R.; Chen, W.; Simpson, T. Comparative studies of metamodelling techniques under multiple modelling criteria. *Struct. Multidiscip. Optim.* **2001**, *23*, 1–13. https://doi.org/10.1007/s00158-001-0160-4.
24. Negrín, I.; Kripka, M.; Yepes, V. Metamodel-assisted design optimization in the field of structural engineering: A literature review. *Structures* **2023**, *52*, 609–631. https://doi.org/10.1016/j.istruc.2023.04.006.
25. Azarhoosh, Z.; Ghazaan, M.I. A review of recent advances in surrogate models for uncertainty quantification of high-dimensional engineering applications. *Comput. Methods Appl. Mech. Eng.* **2025**, *433*, 117508. https://doi.org/10.1016/j.cma.2024.117508.
26. Stein, M.L. *Interpolation of Spatial Data: Some Theory for Kriging*; Springer Science & Business Media: New York, NY, USA, 2012. https://doi.org/10.1007/978-1-4612-1494-6.
27. LeCun, Y.; Bengio, Y.; Hinton, G. Deep Learning. *Nature* **2015**, *521*, 436–444. https://doi.org/10.1038/nature14539.
28. Hornik, K.; Stinchcombe, M.; White, H. Multilayer feedforward networks are universal approximator. *Neural Netw.* **1989**, *2*, 359–366. https://doi.org/10.1016/0893-6080(89)90020-8.
29. Rumelhart, D.E.; McClelland, J.L.; PDP Research Group. *Parallel Distributed Processing: Explorations in the Microstructure of Cognition*; MIT Press: Cambridge, UK, 1986; Volume 1. https://doi.org/10.7551/mitpress/5236.001.0001.

30. Rumelhart, D.E.; Hinton, G.E.; Williams, R.J. Learning Representations by Back-Propagating Errors. *Nature* **1986**, *323*, 533–536. https://doi.org/10.1038/323533a0.
31. Buhmann, M.D. Radial basis functions. *Acta Numer.* **2000**, *9*, 1–38. https://doi.org/10.1017/S0962492900000015.
32. McKay, M.D.; Beckman, R.J.; Conover, W.J. A Comparison of Three Methods for Selecting Values of Input Variables in the Analysis of Output from a Computer Code. *Technometrics* **1979**, *21*, 239–245. https://doi.org/10.2307/1268522.
33. Catalonia Institute of Construction Technology. BEDEC PR/PCT ITEC Materials Database. Barcelona, Spain. Available online: www.itec.cat (accessed on 12 January 2025).
34. Dirección General de Carreteras. *Obras de Paso de Nueva Construcción: Conceptos Generales*; Ministerio de Fomento, Centro de Publicaciones: Madrid, Spain, 2000. (In Spanish).
35. Lophaven, N.S.; Nielsen, H.B.; Sondergaard, J. MATLAB Kriging Toolbox DACE (Design and Analysis of Computer Experiments) Version 2.0. 2002. Available online: http://www2.imm.dtu.dk/pubdb/p.php?1460 (accessed on 17 January 2025).
36. Kirkpatrick, S.; Gelatt, C.D.; Vecchi, M.P. Optimization by simulated annealing. *Science* **1983**, *220*, 671–680. https://doi.org/10.1126/science.220.4598.671.
37. Medina, J.R. Estimation of incident and reflected waves using simulated annealing. *J. Waterw. Port Coast. Ocean. Eng.* **2001**, *127*, 213–221. https://doi.org/10.1061/(ASCE)0733-950X(2001)127:4(213).
38. Martí, J.V.; Yepes, V.; González-Vidosa, F.; Luz, A. Automated Design of Prestressed Concrete Precast Road Bridges with Hybrid Memetic Algorithms. *Rev. Int. Métodos Numér. Cálc. Diseño Ing.* **2014**, *30*, 145–154. https://doi.org/10.1016/j.rimni.2013.04.010.
39. SETRA. *Ponts-Dalles. Guide de Conception*; Ministère de l'Equipement, du Logement des Transports et de la Mer: Bagneux, France, 1989. (In French).